ELSEVIER

NeuroImage

www.elsevier.com/locate/ynimg
NeuroImage 28 (2005) 500 – 506

Technical Note

Concurrent CBF and CMRGlc changes during human brain activation by combined fMRI–PET scanning

Andrew B. Newberg,[a,b,d,*] Jiongjiong Wang,[a,d] Hengyi Rao,[c] Randel L. Swanson,[a] Nancy Wintering,[a] Joel S. Karp,[a] Abass Alavi,[a] Joel H. Greenberg,[c,d] and John A. Detre[a,c,d]

[a]*Department of Radiology, University of Pennsylvania Health System, Philadelphia, PA 19104, USA*
[b]*Department of Psychiatry, University of Pennsylvania Health System, Philadelphia, PA 19104, USA*
[c]*Department of Neurology, University of Pennsylvania Health System, Philadelphia, PA 19104, USA*
[d]*Center for Functional Neuroimaging, University of Pennsylvania Health System, Philadelphia, PA 19104, USA*

Received 22 March 2005; revised 2 June 2005; accepted 10 June 2005
Available online 3 August 2005

A novel approach for concurrent measurement of regional cerebral blood flow (CBF) and regional cerebral metabolic rate for glucose consumption (CMRGlc) in humans is proposed and validated in normal subjects during visual stimulation. ^{18}F-labeled fluorodeoxyglucose was administered during the measurement of CBF by continuous arterial spin labeled magnetic resonance imaging (MRI). Subsequent positron emission tomographic (PET) scanning demonstrated the distribution of labeled deoxyglucose during the MRI acquisition. An excellent concordance between regional CBF and regional CMRGlc during visual stimulation was found, consistent with previously published PET findings. Although initially validated using a brief, non-quantitative protocol, this approach can provide quantitative CBF and CMRGlc, with a broad range of potential applications in functional physiology and pathophysiology.

Introduction

Functional brain imaging has contributed to a greater understanding of regional brain function at rest, during normal sensorimotor and cognitive function, and in disease states. At present, most functional imaging methods measure changes in regional cerebral blood flow (CBF) or metabolism that are coupled to changes in regional brain function. Positron emission tomography (PET) methods are capable of measuring CBF, cerebral blood volume (CBV), cerebral glucose metabolism (CMRGlc), and cerebral oxygen metabolism ($CMRO_2$). These measurements can be made sequentially, but not concurrently. Magnetic resonance imaging (MRI) methods are capable of measuring CBF, CBV, and a complex interaction between blood flow, blood volume, and oxygen utilization termed blood oxygenation level dependent (BOLD) contrast (Ogawa et al., 1992). CBF is measured in MRI using either dynamic susceptibility (Belliveau et al., 1991) contrast or arterial spin labeling (Detre et al., 1992). Arterial spin labeled perfusion MRI utilizes magnetically labeled arterial blood water as an endogenous flow tracer that is directly analogous to $^{15}O-H_2O$ used in PET measurements of cerebral blood flow. Magnetic resonance spectroscopy (MRS) can also be used to measure regional brain metabolism by detecting the fate of exogenously administered isotopic substrates (Zhu et al., 2001; Morris and Bachelard, 2003; Shulman et al., 2004).

In pathological conditions such as stroke, epilepsy, brain tumors, and degenerative diseases, resting alterations in regional blood flow and metabolism detected by PET and MRI have contributed to clinical diagnosis and management. In particular, regional glucose utilization measured by FDG-PET is now an accepted diagnostic test for brain tumor recurrence (increased utilization), lateralization of temporal lobe epilepsy (ipsilateral interictal hypometabolism), and Alzheimer's disease (temporoparietal hypometabolism). Functional MRI (fMRI) with BOLD contrast is readily detected with relatively high spatial and temporal resolution, and is widely used for detecting changes in regional brain activation in response to sensorimotor and cognitive tasks, but does not provide a robust resting measure. Over the past decade, there has been a marked expansion in the use of functional imaging in basic and clinical neuroscience due to the ease and widespread availability of fMRI, which does not require intravenous access, arterial sampling, radioactive isotopes, or a cyclotron.

While a tight coupling between regional neural activity and changes in blood flow and metabolism has been recognized for over a century (Roy and Sherrington, 1890), the exact mechanism for this coupling remains uncertain. Seminal work in the 1980s using multimodal PET scanning demonstrated changes in blood

* Corresponding author. Division of Nuclear Medicine, 110 Donner Building, H.U.P., 3400 Spruce Street, Philadelphia, PA 19104, USA. Fax: +1 215 349 5843.
E-mail address: andrew.newberg@uphs.upenn.edu (A.B. Newberg).
Available online on ScienceDirect (www.sciencedirect.com).

1053-8119/$ - see front matter © 2005 Elsevier Inc. All rights reserved.
doi:10.1016/j.neuroimage.2005.06.040

flow, glucose utilization, and oxygen consumption during functional activation in humans (Fox and Raichle, 1986; Fox et al., 1988). Over the ensuing decades, there has been a continuing effort to gain a better understanding of the physiology of functional activation and the relationship between the measurable parameters in functional neuroimaging and neural activity. Measurements of brain metabolism at rest and during task activation in animal models have demonstrated close correlations between regional brain activity and oxidative metabolism (Smith et al., 2002) and BOLD signal changes (Logothetis et al., 2001), though the cellular compartmentalization of these phenomena are still being investigated (Magistretti and Pellerin, 1999; Kasischke et al., 2004). fMRI measurements of oxygen metabolism require calibrated approaches that are primarily applicable to detecting changes with task activation, and add complexity to investigations in human subjects. Hemodynamic effects are much more readily quantified both at rest and with functional activation using MRI, but their relationship to metabolic substrate utilization is less well characterized, particularly in pathological states.

Here, we report the development and initial validation of a method for concurrent, multimodal measurement of CBF and glucose utilization. In this approach, FDG is administered to subjects during the acquisition of ASL perfusion MRI data. Because FDG is trapped in the brain during the course of its metabolism and has a half-life of 109 min, subsequent PET scanning reflects glucose utilization in the minutes following administration. Initial feasibility is demonstrated using a brief, semi-quantitative protocol during photic stimulation; however, fully quantitative studies are also possible. Task activation used an extremely well-characterized paradigm of alternating checkerboard visual stimulation at 8 Hz. The scanning protocol began with BOLD fMRI using a blocked paradigm with 1-min blocks of visual stimulation alternating with 1 min of fixation. Subsequently, ASL perfusion MRI was measured during 10 min of fixation. Finally, a 10-min ASL perfusion MRI scan was carried out during visual stimulation. At the beginning of this acquisition, the subject was injected with FDG. Once the 10-min scan was completed, subjects were removed from the MRI scanner and moved to the PET scanner to measure regional FDG accumulation, which was carried out from 30 to 60 min following the injection. To assess CMRGlc changes with visual stimulation, a resting PET scan was carried out on a separate day using a similar stimulation protocol but outside the MRI scanner. Arterial blood samples were not acquired for this component of the study, but could easily be performed during the fMRI. Arterial activity curves could then be generated to obtain absolute quantification of the cerebral glucose metabolism.

Materials and methods

Overview of protocol

All subjects provided informed consent using a protocol approved by the institutional review board, the radiation safety committee, and the oversight committee for MRI studies. On the day of the fMRI study, subjects first had an intravenous catheter inserted and were then brought to the MRI scanner and placed in the magnet. An initial anatomical scan was performed for coregistration between the fMRI and PET scans. The subject then underwent BOLD imaging while having their eyes open looking at a fixation point or an 8-Hz alternating checkerboard pattern for 1 min each for five cycles or a total of 10 min. Subjects were then instructed to keep their eyes closed in order to undergo baseline imaging using ASL for 10 min. This was to represent the comparable baseline compared to the baseline FDG-PET scan. A second ASL scan was then performed through a 10-min period where the subject watched the flashing checkerboard. As soon as the checkerboard pattern was initiated, FDG was injected through the intravenous line. After the 10-min fMRI scan, subjects were able to move about and were brought to the Nuclear Medicine Department to undergo the activation PET scanning. Subjects were then placed in the PET scanner and scanned for 30 min in order to compare the activation FDG-PET scan to the activation ASL scan. For the baseline FDG-PET scan, subjects had an intravenous catheter inserted approximately 15 min prior to injection of the FDG. Blood glucose was checked to make certain it was less than 120 mg/dl. Subjects were then injected with the FDG and kept in the baseline state for 10 min after which they could move about. Thirty minutes after injection of the FDG, subjects underwent PET scanning for 30 min.

MR imaging

MR image acquisition was performed on a Siemens 3.0-T Trio whole-body scanner (Siemens AG, Erlangen, Germany), using a standard Transmit/Receive head coil. Disposable ear plugs were provided to reduce the noise of the scanner during operation. Subjects viewed the visual stimulation through a reflective optical system mounted on the head coil. Anatomical scanning consisted of a 3D MPRAGE sequence with TR = 1620 ms, TI = 950 ms, TE = 3 ms, flip angle = 15°, 160 contiguous slices of 1.0 mm thickness, FOV = 192 × 256 mm^2, matrix = 192 × 256, 1NEX with a total scan time of 6 min. BOLD fMRI data were acquired using a gradient-echo EPI sequence, with the imaging parameters of FOV = 192 mm, matrix = 64 × 64, TR = 3 s, TE = 30 ms, flip angle = 75°. Forty contiguous slices (3 mm thickness) were acquired in an interleaved order. The BOLD fMRI scan with 200 acquisitions took 10 min. Continuous arterial spin labeling (CASL) perfusion MRI was performed with a 0.16 G/cm gradient and 22.5 mG RF irradiation applied 8 cm beneath the center of the acquired slices. Control pulse was an amplitude modulated version of the labeling pulse based on a sinusoid function (Wang et al., 2005). The tagging/control duration was 2 s. Interleaved images with and without labeling were acquired using a gradient echo echo-planar imaging (EPI) sequence. A delay of 1 s was inserted between the end of the labeling pulse and image acquisition to reduce transit artifact. Acquisition parameters were: FOV = 22 cm, matrix = 64 × 64, TR = 4 s, TE = 17 ms, flip angle = 90°. Twelve slices (6 mm thickness with 1.5 mm gap) were acquired from inferior to superior in a sequential order. Each CASL scan with 150 acquisitions took 10 min.

PET imaging

Scan acquisition initially required all subjects to have an intravenous catheter. Approximately 0.14 mCi/kg of FDG was injected through the intravenous line immediately at the beginning of the visual stimulation fMRI scan or while the subject was supine in a dark room for the resting condition. PET imaging was initiated 30 min after injection of FDG. The PET data were acquired on a

dedicated G-PET brain scanner based on a GSO detector that operates without septae to increase the sensitivity of the instrument (Karp et al., 2003). At the center of the axial field-of-view, the resolution is 4 mm in the transverse direction and 5 mm in the axial direction. The PET studies were acquired according to protocols developed and validated in our institution. The emission data were reconstructed with a 3D row action maximum likelihood algorithm, which is a fully iterative algorithm. The images are reconstructed into a 128 × 128 × 128 image matrix with voxels of 2 mm × 2 mm × 2 mm.

PET and MR image analysis

PET and MR imaging data processing and analysis were carried out primarily with the Statistical Parametric Mapping software (SPM99, Wellcome Department of Cognitive Neurology, UK implemented in Matlab 5, Math Works, Natick, MA). For each subject, image preprocessing was conducted including realignment, perfusion weighted image construction, coregistration, normalization, and smoothing. MR image series and PET images were realigned to correct for motion. Perfusion weighted image series were generated by pair-wise subtraction of the label and control images, followed by conversion to absolute CBF image series based on a single compartment CASL perfusion model. MR BOLD and quantified CBF images during the visual stimulation and the baseline were averaged to produce one single mean image for each condition. Images of baseline and stimulation were realigned and coregistered with the anatomical image. All functional images were normalized to a 2 × 2 × 2 mm^3 Montreal Neurological Institute (MNI) template using bilinear interpolation and spatially smoothed using a Gaussian filter with a full-width at half maximum (FWHM) parameter set to 5 mm. Then, PET, CBF, and BOLD images were statistically analyzed in the following three steps.

Firstly, to compare the regional CMRGlc and regional CBF signals during 10 min visual stimulation, both the direct average and the SPM group statistical analysis were applied to the concurrent measured PET and CBF images after the global activity for each modality and each subject was corrected by the grand mean scaling of the signal intensity of gray matter. Although CBF at baseline and with visual stimulation was measured quantitatively with MRI, intensity normalization of gray matter values to an arbitrary mean value of 50 was carried out to facilitate comparison with the non-quantitative PET results. This normalization does not affect the quantification of the relative regional CBF data from MRI, but does assume a global coupling between measures. That such a coupling exists in the normal brain seems reasonable and has been demonstrated in previous animal models (Kuschinsky, 1990). Areas showing significant difference between PET and CBF images were identified at the cluster level with a height threshold of uncorrected $P < 0.005$ and an extend threshold of larger than 30 voxels.

Secondly, to reveal the activation induced by the visual stimuli, the SPM group statistical analysis was defined as 'Population main effect (paired t test)' and applied to the three kinds of functional images of 5 subjects during visual stimulation and baseline. Voxel-wise analysis of the PET, CBF, and BOLD data was conducted to identify voxels with a significant response to the visual stimulation relative to the baseline according to the general linear model. Areas of significant activation were identified at the cluster level with a height threshold of uncorrected $P < 0.05$ and an extend threshold of larger than 500 voxels.

Finally, a region of interest (ROI) analysis was conducted to calculate the signal increases of regional CMRGlc, regional CBF, and BOLD induced by visual stimuli and estimate the consistency of activations across three modalities. Primary visual cortex (bilateral calcarine area) was defined as the ROI from an automated anatomical labeling ROI library (Tzourio-Mazoyer et al., 2002) in the SPM Marsbar toolbox. For each subject, the visual stimulus-induced signal increases in the ROI were calculated by subtracting the signal intensity during baseline from the signal intensity during visual stimulation and dividing by the signal intensity during baseline. The activation centroids of three modalities were calculated by the weighted sum of the signal increases and the MNI coordinate of each voxel showing signal increasing in the primary visual cortex.

To correct relative CMRGlc for the 10-min activation protocol, an operational equation for cerebral glucose utilization was used in which the metabolic rate is assumed to be MR_1 from $t = 0$ to $t = t_1$, and MR_2 from $t = t_1$ to $t = t_2$.

$$MR_1 = [C(t_2) - CE(t_2)]/L \times S_{01} - [S_{12}/S_{01}]MR_2 \quad (1)$$

where $C(T)$ = tissue concentration of FDG at scan time (t_2); L = lumped constant of FDG; $CE(T)$ = unmetabolized tracer at scan time; S_{01} = integrated specific activity input to tissue from $t = 0$ to $t = t_1$; S_{12} = integrated specific activity input to tissue from $t = t_1$ to $t = t_2$.

For a region of interest equation (R) and whole brain (B), Eq. (1) becomes:

$$^{R}MR_1 = \left[^{R}C(t_2) - CE(t_2)\right]/L \times S_{01} - [S_{12}/S_{01}]^{R}MR_2 \quad (2)$$

$$^{B}MR_1 = \left[^{B}C(t_2) - CE(t_2)\right]/L \times S_{01} - [S_{12}/S_{01}]^{B}MR_2. \quad (3)$$

Assuming that at time of PET scan (t_2), that $CE(t_2) = 0.15\ ^{B}C(t_2)$. Eqs. (2) and (3) become:

$$^{R}MR_1 = \left[0.85^{R}C(t_2)\right]/L \times S_{01} - [S_{12}/S_{01}]^{R}MR_2 \quad (4)$$

$$^{B}MR_1 = \left[0.85^{B}C(t_2)\right]/L \times S_{01} - [S_{12}/S_{01}]^{B}MR_2. \quad (5)$$

Rearranging Eqs. (4) and (5), and dividing, letting $S = S_{12} / S_{01}$:

$$\left[^{R}MR_1 + S^{R}MR_2\right]/\left[^{B}MR_1 + S^{B}MR_2\right] = {}^{R}C(t_2)/{}^{B}C(t_2). \quad (6)$$

Under conditions of no visual stimulation (control FDG scan), $^{B}MR_1 = {}^{B}MR_2$, and Eq. (6) becomes:

$$^{R}MR_2/{}^{B}MR_2 = {}^{R}C(t_2)'/{}^{B}C(t_2)'$$
$$= \text{ratio of tissue concentrations (no stimulation)}. \quad (7)$$

Combining Eqs. (6) and (7) results in the following equation:

$$^{R}MR_1/{}^{B}MR_1 = {}^{R}C(t_2)/{}^{B}C(t_2) + S\left[^{B}MR_2/{}^{B}MR_1\right] \times \left[^{R}C(t_2)/{}^{B}C(t_2) - {}^{R}C(t_2)'/{}^{B}C(t_2)'\right]. \quad (8)$$

This equation states that the ratio of the metabolic rate in region of interest (R) to the metabolic rate in the whole brain (B) equals the ratio of the tissue concentrations during visual stimulation plus the ratio of the integrated specific activity inputs from $t = 0$ to $t = t_1$ and from $t = t_1$ to $t = t_2$ times the ratio of the metabolic rates for region R and whole brain during a control (no stimulus scan) times

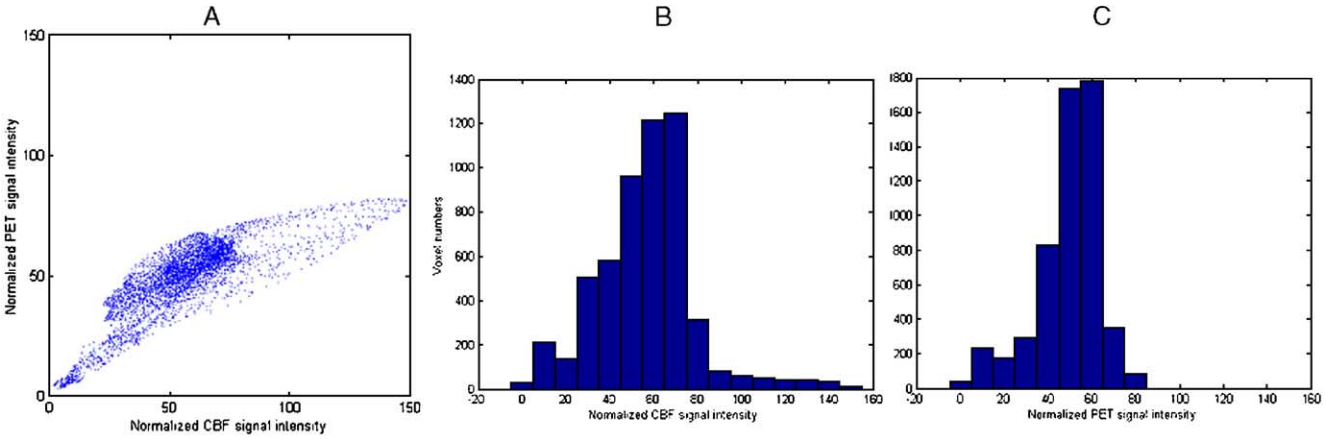

Fig. 1. Plots of mean normalized PET and CBF signal distributions during visual stimulation (at the slice of $Z = 0$, excluding the voxels outside the brain). (A) Plot of normalized PET signal intensity against normalized CBF signal intensity ($r = 0.83$, $P < 0.0001$). (B) Histogram of normalized PET signal intensity. (C) Histogram of normalized CBF signal intensity. PET and CBF values were normalized to an arbitrary whole brain mean value of 50.

the difference in tissue concentration ratios during stimulus and during no stimulus. All of these parameters are known so that a correction for functional measures can be made for the situation where the visual stimulus is not performed for the entire study.

Results

Five subjects completed the scanning protocol. Group results and individual activation within a region of interest (ROI) in primary visual cortex were compared for each modality following coregistration and normalization of global intensities. Fig. 1 shows a histogram plot of normalized values for a representative single brain slice at $Z = 0$. The figure shows that there is a strong correlation between normalized CBF and CMRGlc values and that they are similarly distributed (although the CBF data is more broadly distributed). However, at higher flow rates, there is a relative plateau of metabolic values versus CBF. This might be accounted for by differences in processing of quantitative CBF and qualitative CMRGlc data, artifactual overestimation of regional CBF, or by an actual physiological difference. Future quantitative studies will be needed in order to determine the validity of this finding.

Fig. 2 shows group results comparing mean normalized CBF and CMRGlc measured concurrently during visual stimulation, as well as the results of a statistical comparison of significant differences between the MRI and PET results. The normalized CBF data show greater relative intensity in visual cortex than does the CMRGlc data (Fig. 2B versus Fig. 2A). This is reflected in the statistical comparison (Fig. 2C), which shows a significant increase in ASL MRI versus FDG-PET in visual cortex (blue), whereas FDG-PET shows significantly greater signal than ASL MRI in basal ganglia (red). This latter finding may reflect task differences, an uncoupling between CBF and CMRGlc in this region,

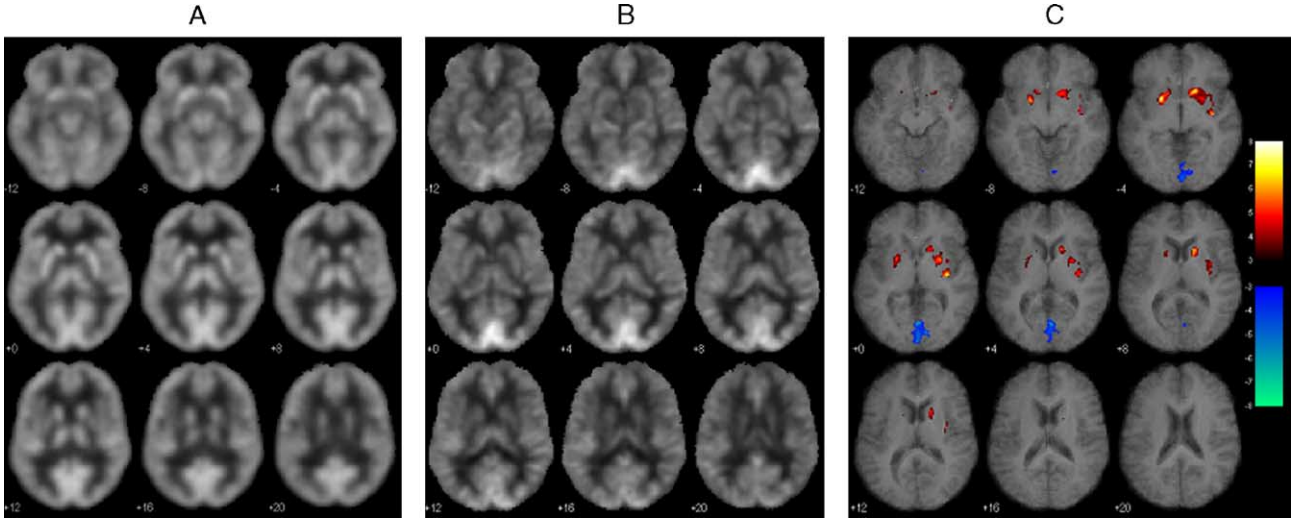

Fig. 2. Group results comparing (A) relative cerebral glucose metabolism (CMRGlc) and (B) cerebral blood flow (CBF) by FDG-PET and ASL-perfusion fMRI during visual stimulation from 5 subjects. (C) Results of the SPM group analysis of the contrast between CMRGlc and CBF (two sample t test, uncorrected $P < 0.005$, extent threshold $k > 30$ voxels). Note CMRGlc showed higher signal in bilateral basal ganglia (red) and CBF showed higher signal in visual cortex (blue).

inaccuracies in the model used to correct for the fact that the visual stimulus in the PET study did not extend for the same length as it did for the MRI study, or potential inaccuracies in image processing and attenuation correction. This latter possibility may relate to the normalization process which assumes similar signal-to-noise ratios between the fMRI and PET data. To account for potential differences, a two-sample t test was used to produce Fig. 2C. Hence, the differences observed between CBF and CMRGlc more likely reflect a physiological effect.

Fig. 3 compares results of visual stimulation versus rest for PET, ASL perfusion MRI, and BOLD contrast at a statistical threshold of uncorrected $P < 0.05$ for activation clusters exceeding 500 voxels. For these results, resting PET data were acquired in a separate session, whereas ASL and BOLD MRI data during both rest and activation were acquired in the same scanning session. There is substantial concordance between these maps. PET activation includes a region of suprathreshold activation in right auditory cortex not seen in ASL or BOLD MRI, which may reflect effects of MRI scanner noise that was present during the PET activation study but not the separate resting PET study performed outside of the MRI scanner.

The results of the ROI analysis for primary visual cortex are presented in Table 1. Percent increases in CBF and CMRGlc are comparable at 28.3 ± 16% and 24.4 ± 18%, respectively (N.S.) for the group, but with considerable variability across individuals, particularly in FDG-PET results. When subjects were considered as a group, the variability of the CBF seemed relatively equivalent to that of FDG. Much of this variability may be attributable to the use of a non-quantitative PET approach for this initial feasibility study. Quantitative CBF values within the same ROI were 58 ± 6.4 ml/100 g/min at rest and 71 ± 12 ml/100 g/min with visual stimulation. BOLD signal change was 1.0 ± 0.5% in the same ROI. The activation centroids for each modality are listed in Table 2. Activation centroids were about 10 mm distance from each other, with no significant intermodality differences, though the smallest difference was observed intramodally between ASL and BOLD MRI.

Table 1
The visual-stimuli-induced signal increases between the activation of CMRGlc, CBF, and BOLD in the primary visual cortex of each subject

	CMRGlc signal increase% (peak%)[a]	CBF signal increase% (peak)	BOLD signal increase% (peak)
Subject 1	47.4 (267.5)	9.1 (225.0)	0.3 (12.4)
Subject 2	−2.1 (425.7)	45.8 (316.7)	0.8 (10.2)
Subject 3	26.7 (127.2)	17.0 (100.1)	1.7 (8.6)
Subject 4	29.9 (217.3)	41.4 (382.9)	1.0 (6.5)
Subject 5	20.3 (238.5)	28.3 (233.3)	1.1 (13.9)
Mean ± SD	24.4 ± 17.9 (255.2 ± 108.8)	28.3 ± 15.6 (251.6 ± 106.6)	1.0 ± 0.5 (10.3 ± 2.9)

[a] PET signal changes were calculated after the correction of 10-min visual stimulation and 30-min interval between the injection of FDG and PET imaging.

Discussion

These results demonstrate the feasibility of obtaining concurrent CBF and CMRGlc using a combined fMRI–PET approach. The close agreement in the magnitude and spatial localization of CBF and CMRGlc in visual cortex during visual stimulation measured using this approach is in agreement with previously published PET results (Fox and Raichle, 1986). Differences in the

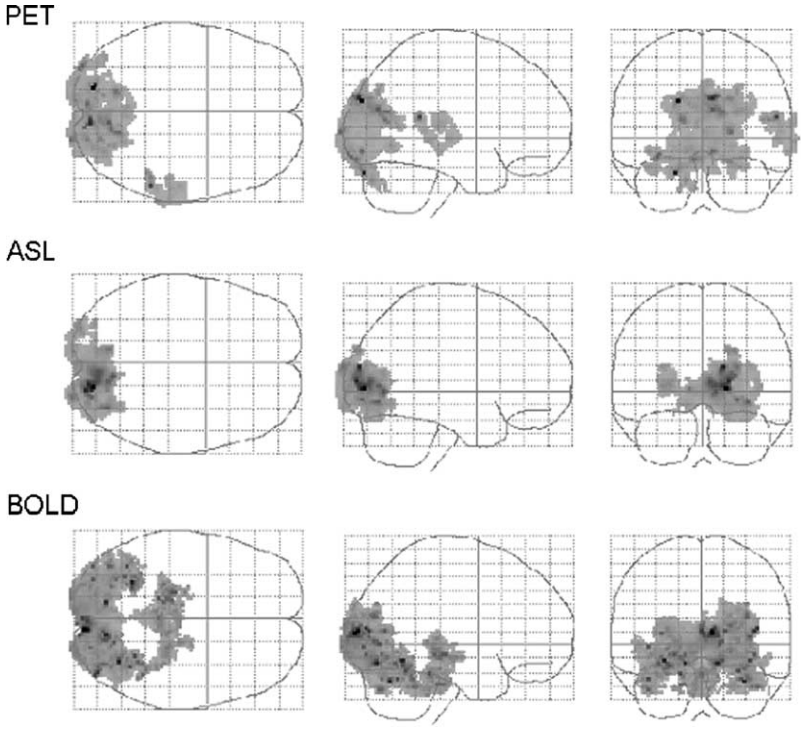

Fig. 3. SPM{t} maps from the group analysis of the contrast between visual stimulation and baseline (paired t test, uncorrected $P < 0.05$, extent threshold $k >$ 500 voxels) for FDG-PET (top), ASL perfusion fMRI (middle), and BOLD fMRI (bottom).

Table 2
The activation centroids (MNI coordinates) of CMRGlc, CBF, and BOLD and the distances (mm) between these centroids in the primary visual cortex of each subject

	CMRGlc centroid	CBF centroid	BOLD centroid	CBF–CMRGlc distance	CBF–BOLD distance	CMRGlc–BOLD distance
Subject 1	[3.4, −77.5, 6.5]	[4.7, −85.8, 1.9]	[3.6, −90.2, 2.9]	9.57	4.62	13.19
Subject 2	[2.4, −80.9, 5.1]	[2.3, −91.6, 0.2]	[1.1, −90.0, 0.3]	11.75	2.04	10.33
Subject 3	[2.4, −85.7, 3.8]	[4.7, −85.9, 4.0]	[1.3, −87.8, 2.6]	2.29	4.17	2.67
Subject 4	[3.0, −76.5, 6.7]	[2.4, −90.3, 1.4]	[1.4, −88.8, 1.5]	14.80	1.85	13.41
Subject 5	[2.9, −78.6, 6.1]	[3.3, −90.5, −0.8]	[1.9, −88.4, −0.1]	13.76	2.70	11.56
Mean (SD)	[2.8, −79.8, 5.6] (0.4, 3.7, 1.2)	[3.5, −88.8, 1.3] (1.2, 2.8, 1.8)	[1.9, −89.0, 1.4] (1.0, 1.0, 1.3)	10.43 (4.97)	3.08 (1.25)	10.23 (4.41)

magnitude of CBF and CMRGlc changes between the two studies are likely attributable to differences in the regions over which these changes were averaged. The differences in the areas and extent of activation might also be attributable to the normalization process of both the fMRI and PET data which assumes a global coupling and a similar signal-to-noise contrast. Further refinements of combined fMRI–PET method will include the addition of arterial blood sampling to allow CMRGlc to be quantified in absolute values, and the use of higher-resolution fMRI scanning to allow the spatial distribution of changes in CBF and CMRGlc to be examined in greater detail. Subtle differences in the spatial distribution of CBF and CMRGlc changes with visual stimulation are suggested in Fig. 1C, though these require further verification with a quantitative approach, including careful consideration of attenuation correction for the apparent differences seen in basal ganglia (Hoffman et al., 1991). The temporal resolution of this combined fMRI–PET is limited by the rate of brain uptake and metabolism of fluorodeoxyglucose, which requires many minutes. While relatively long scanning times are not problematic for resting studies in controls versus pathological states or for pharmacological effects, future studies will be needed to determine the optimum duration for combined fMRI–PET studies of task activation. Perfusion fMRI has been shown to be sensitive at extremely low task frequencies (Aguirre et al., 2002, Wang et al., 2003) and is ideally suited to this combined approach.

Although CBF and CMRGlc can be obtained with sequential PET measurements with the availability of ^{15}O radiopharmaceuticals, there are several applications in which concurrent measurements would be highly desirable. For detailed studies of functional physiology in awake human subjects in whom behavioral states such as anxiety or attention could affect the reproducibility of sequential stimulus conditions, the ability to measure CBF and CMRGlc simultaneously should strengthen the inferences that can be drawn from the data, the resolution of which could be considerably higher than what was available when this topic was initially addressed in the 1980s. Concurrent CBF and CMRGlc would also provide the most reliable means of validating MRI-based alternatives to clinical FDG-PET, as both modalities could be examined under identical conditions. This would be particularly important for applications in epilepsy, where spontaneous fluctuations in CBF and metabolism in affected regions are expected, though alterations in regional CBF and metabolism may also occur in other neuropsychiatric conditions if the behavioral or pharmacological state of the patient is not well controlled. Concurrent measures would also be valuable in pathological states in which the coupling between CBF and metabolism is affected or could fluctuate, and in situations where experimental conditions are difficult to reproduce. For example, alterations in the flow response to functional activation are well documented following stroke (Pineiro et al., 2002; Grohn and Kauppinen, 2001), and the ability to precisely correlate changes in flow and metabolism in stroke recovery would help validate the use of flow-based imaging such as fMRI in characterizing stroke recovery. Caffeine reduces baseline CBF (Laurienti et al., 2002; Mulderink et al., 2002; Dager and Friedman, 2000), yet is an effective stimulant, suggesting a functionally paradoxical uncoupling of CBF and metabolism. Studies of caffeine effects on performance and brain function following chronic sleep deprivation require an enormous investment in subject preparation that is not readily repeated, and serves as another motivation for the development of this method.

In summary, we demonstrate the feasibility of concurrent measurements of CBF and CMRGlc with combined fMRI–PET. Simple improvements in experimental design such as longer task conditions and arterial blood sampling should lead to an quantitative approach that will allow accurate correlations between CBF and metabolism at high spatial resolution and without the need for a cyclotron. This method can be readily implemented in any center with both fMRI and PET capabilities.

Acknowledgments

This research was supported in part by the following grants: NIH-NS045839, NIH-RR02305, and a grant from the Counter Drug Technology Assessment Center. We would also like to thank the MRI and PET Center personnel for their assistance with this study.

References

Aguirre, G.K., Detre, J.A., Zarahn, E., Alsop, D.C., 2002. Experimental design and the relative sensitivity of BOLD and perfusion fMRI. NeuroImage 15, 488–500.

Belliveau, J.W., Kennedy, D.W., McKinstry, R.C., Buchbinder, B.R., Weisskoff, R.M., Cohen, M.S., Vevea, J.M., Brady, T.J., Rosen, B.R., 1991. Functional mapping of the human visual cortex by magnetic resonance imaging. Science 254, 716–718.

Dager, S.R., Friedman, S.D., 2000. Brain imaging and the effects of caffeine and nicotine. Ann. Med. 32, 592–599.

Detre, J.A., Leigh, J.S., Williams, D.S., Koretsky, A.P., 1992. Perfusion imaging. Magn. Reson. Med. 23, 37–45.

Fox, P.T., Raichle, M.E., 1986. Focal physiological uncoupling of cerebral blood flow and oxidative metabolism during somatosensory stimulation in human subjects. Proc. Natl. Acad. Sci. U. S. A. 83, 1140–1144.

Fox, P.T., Raichle, M.E., Minutun, M.A., Dence, C., 1988. Nonoxidative glucose consumption during focal physiological neural activity. Science 241, 462–464.

Grohn, O.H., Kauppinen, R.A., 2001. Assessment of brain tissue viability in acute ischemic stroke by BOLD MRI. NMR Biomed. 14, 432–440.

Hoffman, E.J., Cutler, P.D., Guerrero, T.M., Digby, W.M., Mazziotta, J.C., 1991. Assessment of accuracy of PET utilizing a 3-D phantom to simulate the activity distribution of [18F]fluorodeoxyglucose uptake in the human brain. J. Cereb. Blood Flow Metab. 11, A17–A25.

Karp, J.S., Surti, S., Daube-Witherspoon, M.E., Freifelder, R., Cardi, C.A., Adam, L.E., Bilger, K., Muehllehner, R.G., 2003. Performance of a brain PET camera based on anger-logic gadolinium oxyorthosilicate detectors. J. Nucl. Med. 44, 1340–1349.

Kasischke, K.A., Vishwasrao, H.D., Fisher, P.J., Zipfel, W.R., Webb, W.W., 2004. Neural activity triggers neuronal oxidative metabolism followed by astrocytic glycolysis. Science 305, 99–103.

Kuschinsky, W., 1990. Coupling of blood flow and metabolism in the brain. J. Basic Clin. Physiol. Pharmacol. 1, 191–201.

Laurienti, P.J., Field, A.S., Burdette, J.H., Maldjian, J.A., Yen, Y.F., Moody, D.M., 2002. Dietary caffeine consumption modulates fMRI measures. NeuroImage 17, 751–757\

Logothetis, N.K., Pauls, J., Augath, M., Trinath, T., Oeltermann, A., 2001. Neurophysiological investigation of the basis of the fMRI signal. Nature 412, 150–157.

Magistretti, P.J., Pellerin, L., 1999. Cellular mechanisms of brain energy metabolism and their relevance to functional brain imaging. Philos. Trans. R. Soc. Lond., Ser. B Biol. Sci. 354, 1155–1163.

Morris, P., Bachelard, H., 2003. Reflections on the application of 13C-MRS to research on brain metabolism. NMR Biomed. 16, 303–312.

Mulderink, T.A., Gitelman, D.R., Mesulam, M.M., Parrish, T.B., 2002. On the use of caffeine as a contrast booster for BOLD fMRI studies. NeuroImage 15, 37–44.

Ogawa, S., Tank, D.W., Menon, R., Ellermann, J., Kim, S.-G., Merkle, H., Ugurbil, K., 1992. Intrinsic signal changes accompanying sensory stimulation: functional brain mapping with magnetic resonance imaging. Proc. Natl. Acad. Sci. U. S. A. 89, 5951–5955.

Pineiro, R., Pendlebury, S., Johansen-Berg, H., Matthews, P.M., 2002. Altered hemodynamic responses in patients after subcortical stroke measured by functional MRI. Stroke 33, 103–109.

Roy, C.S., Sherrington, C.S., 1890. On the regulation of the blood-supply of the brain. J. Physiol. 11, 85–108.

Shulman, R.G., Rothman, D.L., Behar, K.L., Hyder, F., 2004. Energetic basis of brain activity: implications for neuroimaging. Trends Neurosci. 27, 489–495.

Smith, A.J., Blumenfeld, H., Behar, K.L., Rothman, D.L., Shulman, R.G., Hyder, F., 2002. Cerebral energetics and spiking frequency: the neurophysiological basis of fMRI. Proc. Natl. Acad. Sci. U. S. A. 99, 10765–10770.

Tzourio-Mazoyer, N., Landeau, B., Papathanassiou, D., Crivello, F., Etard, O., Delcroix, N., Mazoyer, B., Joliot, M., 2002. Automated anatomical labelling of activations in SPM using a macroscopic anatomical parcellation of the MNI MRI single subject brain. NeuroImage 15, 273–289.

Wang, J., Aguirre, G.K., Kimberg, D.Y., Roc, A.C., Li, L., Detre, J.A., 2003. Arterial spin labeling perfusion fMRI with very low task frequency. Magn. Reson. Med. 49, 796–802.

Wang, J., Zhang, Y., Wolf, R.L., Roc, A.C., Alsop, D.C., Detre, J.A., 2005. Amplitude modulated continuous arterial spin-labeling 3.0-T perfusion MR imaging with a single coil: feasibility study. Radiology 235, 218–228.

Zhu, X.H., Merkle, H., Kwag, J.H., Ugurbil, K., Chen, W., 2001. 17O relaxation time and NMR sensitivity of cerebral water and their field dependence. Magn. Reson. Med. 45 (4), 543–549.